

Numerical Simulation of Mixing Performance on the Rotating Electroosmotic Micromixer

Mohammad Reza Shahnazari^{1,*}, Hamid Chenarani¹, Jahan B. Ghasemi², and Ali J. Chamkha³

¹Department of Mechanical Engineering, K. N. Toosi University of Technology, Tehran, Iran

²Department of Chemistry, University College of Science, University of Tehran, Tehran, Iran

³Faculty of Engineering, Kuwait College of Science and Technology, Doha District, 35004, Kuwait

Lab-on-a-disk systems have become popular during the past two decades by accelerating the biomedical diagnostic process and chemical reactions. Mixing performance should be attended to because of its importance in lab-on-a-disk systems. This paper investigates applying a voltage to the mixing performance in a centrifugal serpentine three-dimensional micromixer. The finite element method is used for the simulation-based COMSOL Multiphysics 5.6 program. Working fluid has the same properties as water in 298 K. The results indicate that increasing angular velocity causes mixing quality to drop until the threshold angular velocity increases. Also, it is observed that applying an electric field into the domain can improve mixing quality, and as a result, channel length decreases; hence more patterns will be placed on one disk.

KEYWORDS: Micromixers, Electroosmotic, Lab-on-a-Disk, Centrifugal Microfluidics, Electric Fields.

1. INTRODUCTION

By reducing the sample volume, microfluidics has come to the aid of various sciences, which investigate fluid flow behavior through micro-channels and the technology of producing microfluidic devices.¹

Laboratory analyses, including DNA sequencing and biochemical detections, have transitioned to being cost-effective, yielding quicker responses, and requiring smaller sample volumes through the adoption of lab-on-a-chip (LOC) devices. This transformation owes much to the integration of microfluidics and molecular biology, which stand as pivotal and foundational technologies in the advancement of LOC fields.²

In a LOC device, some components, such as micropumps, microvalves, micromixers, etc., are installed to conduct fluid into the chip channels and create the desired reactions.³ However, the LOC device has many drawbacks, such as the difficulty of multiplexing, bubble formation, tubing requirement for fluid pumping, and difficulty handling large volumes.⁴ Centrifugal microfluidic platforms diminish LOC's mentioned problems.⁵

Lab-on-a-disc (LOAD) is a centrifugal microfluidic platform that can contain several operation units such as mixing,⁶ separation,⁷ and valving⁸ simultaneously on a disk. LOAD system has several advantages, such as pump

eliminations, assays on a disk, easy metering, and mixing fluids. The usability of all fluids without considering physical properties and trapped bubbles elimination are some of the other benefits of LOAD.⁹ Despite these advantages, the difficulty of working with less than 1nL and unidirectional fluid flow consider significant drawbacks.⁴

LOAD system contains a motor that generates fluid flow-driven forces, a disk-like CD mounted on the motor shaft, and detection components. Pattern designing of disk microchannels depends on their application, such as point of care (POC) diagnostics,¹⁰ DNA amplification,¹¹ biosensing, and biochemical.^{12, 13}

In microfluidic systems, the flow structure and the conditions governing it are fundamental. In the research, important cases such as various geometry of the cross-section of the channels and conditions such as peristaltic flow and application of peristaltic wave on the microchannel have been investigated. The channel also requires a stimulus for fluid flow, so to improve mixing, the jet is used in two categories: free jet and confined jet. But the loading device does not need an external stimulus for fluid flow.^{14–16}

In all biomedical and biochemical applications, mixing performance has a key role. The fluid flow within the microchannel predominantly operates within the regime of low Reynolds numbers, characterized by laminar flow behavior. Thus, to achieve proper mixing, passive and active micromixer have been used.¹⁷

Passive micromixers have simple structures. They have been preferred more because of no external driver input

*Author to whom correspondence should be addressed.

Email: Shahnazari@kntu.ac.ir

Received: 2 October 2022

Accepted: 31 January 2023

requirement.¹⁸ Ionescu¹⁹ utilized the COMSOL Multiphysics software, which operates on the Finite Element Method (FEM), to analyze the mixing performance within rotating microchannels of the LOCD type, taking into account various cross-sectional dimensions. He investigated seven-channel models with aspect ratios between 2 and 0.67 and hydraulic diameters between 200 and 240 μm . He reported that an appropriate model had an aspect ratio of 0.67 and a hydraulic diameter of 200–222 μm .

Chaotic advection and diffusion are the basis of the passive mixing process.²⁰ In passive micromixers, a mixing operation is performed according to the channel's geometry and structure.²¹ Efficient mixing of two fluids can be achieved by employing a conductive plate with a curved arc shape, as opposed to a flat conductive plate or other non-conductive obstacles, especially when dealing with Newtonian fluids. Goodarzi et al.²² employed this approach. They conducted a comprehensive examination of various factors, including differences in radius curves, span length, the number of curved arc plates situated within the channel, arrangement patterns, concavity direction, and orientation angles, in relation to the flow and mixing process. Babaie et al.,²³ introduced a passive micromixer, which was modified by incorporating convergent-divergent cross sections to enhance mixing efficiency. The modification was implemented with the goal of capitalizing on the concurrent occurrence of Dean vortices and separation vortices. The investigation delved into the influence of both amplitude and wavelength to ascertain the optimal configuration for practical applications of the serpentine-sinusoidal mixer. The researchers concluded that placing convergent and divergent barriers sequentially resulted in the production of stronger Dean vortices, ultimately leading to an elevated level of mixing efficiency.

Conversely, external energy inputs like electric fields, magnetic fields, and similar forces are prerequisites for fluid mixing.²⁰ Although an active micromixer's structure is more complicated and expensive than a passive one's, it has advantages such as a convenient layout, flexible control, and short mixing time.²⁴ According to the currently applied types: Direct current (DC),²⁵ and alternating current (AC),²⁶ fluid flow in electroosmotic micromixers is classified into two categories. One of the most popular designs for passive micromixer channels is a spiral. Park and Kwon²⁷ investigated numerical simulation of mixing performance in a three-dimensional serpentine micromixer (TSM), which channel designed in "L, C, and F" shape mixing units. Experimental and computational simulations indicate that obstacles in serpentine microchannels present better mixing performance and obstacles contain grooves in the channel's wall, microbeads, and baffles.^{28–30} Steigert et al.³¹ introduced centrifugal microfluidic platforms. In LOAD platforms, the Coriolis and Euler forces, known as inertial forces and angular frequency, are essential factors

in mixing. La et al.³² recommend and evaluate a serpentine micromixer in a lab-on-a-disk platform for biochemical assays. They reach acceptable mixing quality by their design which transverse secondary flow and emotional effect play an important role in mixing performance. Shamloo et al.³³ improved the mixing efficiency by modifying the channel curvature in a centrifugal micromixer platform. Their design's mixing quality numbers reported about 90% better than rectilinear and straightforward designs. The channel length is important because more patterns will be placed in a disk by shortening it; therefore, applying magnetic or electric fields into the system can be effective. Xiong et al.³⁴ numerically investigated several electrode pairs on a two-dimensional Koch fractal structure mixing performance. They applied time-dependent sinusoidal alternating current to the electrodes and reported that the number of electrode pairs directly affects mixing quality. A novel three-dimensional Koch fractal structure electroosmotic micromixer was employed by Xiong and Chen.³⁵ They investigate the effects of fractal size, number of electrodes, electrode distance, and voltage range on the mixing efficiency. A straight microchannel contains a rhombus shape chamber in which four electrodes are placed on channel walls employed by Jalili et al.³⁶ They applied a sinusoidal electric field to the channel and investigated mixing performance. Their simulation indicates that mixing time decreases by applying an electrical field, and mixing quality increases.

In this study, the amalgamation of two fluid flows possessing akin physical properties yet distinct concentrations was examined employing the finite element method within the COMSOL 5.6 software. To augment the mixing rate and reduce the channel length, an alternative electric field was administered to the electrodes. The impact of variables such as voltage amplitude, angular velocity, the quantity of electrode pairs, and diverse arrangements of electrode pair distribution was evaluated.

2. THEORETICAL BACKGROUND

2.1. Geometry Principals

The desired micromixer was designed by Shamloo et al.,³³ and in this numerical simulation, four electrodes were applied to it, as shown in Figure 1.

The curvature of the channel design induces the Coriolis force and the Dean effect, resulting in an augmentation of the secondary flow within the channel. This, in turn, leads to an enhancement in mixing efficiency. The electric field applied to the channel follows a time-varying sinusoidal pattern, which accelerates the mixing process, enabling it to occur in a shorter time and over a reduced distance from the inlets.

2.2. Governing Equations and Dimensionless Numbers

Governing equations in this study are classified into three parts related to fluid flow, electric field, and mass transfer.

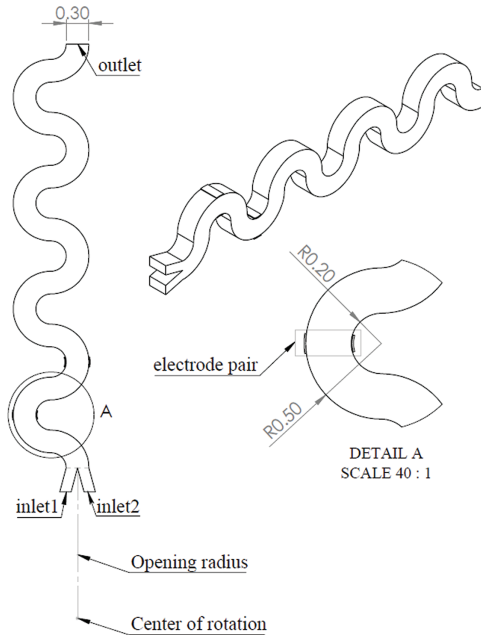


Fig. 1. Schematic geometry of micromixer, dimensions (in mm).

For a Newtonian and incompressible fluid with constant properties, Navier-Stokes momentum and continuity equations govern the flow as:

$$\rho \frac{\partial u}{\partial t} + \rho(u \cdot \nabla)u + \nabla p - \mu \nabla^2 u - f_b = 0 \quad (1)$$

$$\nabla \cdot u = 0 \quad (2)$$

where ρ , u , μ , p , and f_b denote fluid density, velocity vector, dynamic viscosity, pressure, and volumetric force vector. The volumetric force consists of Coriolis and Centrifugal forces and per unit of volume expressed as below.

$$f_b = f_{\text{Centrifugal}} + f_{\text{Coriolis}} = -\rho\omega^2 r - 2\rho\omega u \quad (3)$$

in which ω and r are angular velocity and rotation radius, respectively.

The Convection-Diffusion equation is employed to analyze particle motion and is expressed as follows:

$$\frac{\partial c}{\partial t} + \nabla \cdot (-D\nabla c) = -u \cdot \nabla c \quad (4)$$

where D and c denote diffusion coefficient, which is constant and concentration, respectively.

The current micromixer field is based on Ohm's law expressed as the following equation.

$$\nabla \cdot (-\sigma \nabla V) = 0 \quad (5)$$

where σ and V are conductivity and electric potential, respectively. Finally, $(-\sigma \nabla V)$ the expression represents current density.

Mixing efficiency obtained as:

$$M.Q. = 1 - \sqrt{\frac{1}{N} \sum_{j=1}^N \left(\frac{c_j - \bar{c}}{\bar{c}} \right)^2} \quad (6)$$

in which $M.Q.$, N , c_j , \bar{c} denote mixing quality, total number of sampling points, Normalized concentration, and expected normalized concentration, respectively. The mixing quality can differ from 0 to 1, in which 0 indicates no mixing and 1 denotes full mixing.

The dimensionless Reynolds number (Re) signifies the relationship between inertial forces and viscous forces, providing insight into the regime of fluid flow. Specifically, fluid flow is characterized as laminar at low Reynolds numbers, while it transitions into a turbulent state at higher Reynolds numbers.

$$Re = \frac{\rho \bar{u} D_h}{\mu} \quad (7)$$

in which \bar{u} and D_h are mean velocity and the microchannel's hydraulic diameter.

Hydraulic diameter obtained as:

$$D_h = \frac{4A_c}{p_w} \quad (8)$$

where A_c and p_w denote the channel's cross-section area and wetted perimeter.

In a curved microchannel, Dean number (De) is another dimensionless group that is Reynolds number's product and the curvature ratio's square root.

$$De = Re \sqrt{\frac{D_h}{2R_c}} \quad (9)$$

where R_c is the microchannel's radius of curvature.

2.3. Boundary Conditions

In the study of fluid flow, the microchannel walls were subject to the application of the electroosmotic slip velocity boundary condition. At the same time, constant zero-pressure boundary conditions were imposed at both the inlet and outlet. In this study, one of the simplicity assumptions is omitting the gravity effect. Working fluid has the same properties as deionized water, in which density (ρ), dynamic viscosity (μ), relative permittivity (ϵ_r), constant diffusion coefficient (D), the conductivity of the ionic fluid (σ) are $10^3(\text{kg/m}^3)$, $1 \times 10^{-3}(\text{pa} \cdot \text{s})$, 80.2 , $1.67 \times 10^{-9}(\text{m}^2/\text{s})$, $0.11845(\text{S/M})$, respectively. Concentration at inlet 1 assumed $1(\text{mol/m}^3)$ and at inlet 2 assumed $0(\text{mol/m}^3)$.³³

Helmholtz–Smoluchowsky presented slip velocity as:

$$u_{\text{slip}} = \frac{\epsilon_0 \epsilon_r \xi_0}{\mu} \nabla V \quad (10)$$

where ϵ_0 , ϵ_r and ξ_0 represent the fluid's electric permittivity and zeta potential exerted at walls.

Equation (11) indicates applied alternating current, which is sinusoidal on electrodes and the insulated boundary condition applied on all other boundaries is given as Eq. (12):

$$V = V_0 \sin(2\pi ft + \varphi) \quad (11)$$

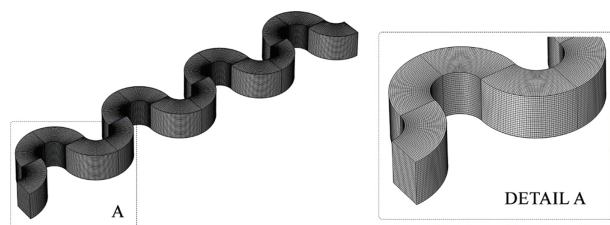


Fig. 2. Structured mesh generation centrifugal force-based serpentine micromixer CSM.

Table I. Variation of mixing quality percentage with down-channel length.

Total cell numbers	M.Q.
167,936	98.9%
288,800	96.1%
441,408	94.4%
660,000	94.1%

$$-\sigma \nabla V \cdot n = 0 \tag{12}$$

in which f is the frequency assumed at 12 Hz and V_0 is the amplitude of the AC potential which equals 5 V.

2.4. Numerical Modeling

The problem was simulated using COMSOL Multiphysics software, version 5.6. The simulation methodology in this software is founded on the finite element method (FEM). To optimize computational efficiency and conserve memory resources, the simulation study is compartmentalized into two distinct stages: stationary and time-dependent. In the initial stage, the physics of fluid flow and chemical species transport are resolved under the specified boundary conditions. The outcomes of this stage serve as the initial values for the subsequent phase. In the second stage, a time-dependent electric field is computed and integrated with the Navier-Stocks and diffusion-convection equations.³⁶

2.4.1. Grid Independence Analysis

Figure 2 depicts a structured mesh used in this study. Grid independence was conducted to achieve good accuracy in the simulation. Four total cell numbers of 167,936, 288,800, 441,408, and 660,000 are used for this analysis. Table I shows the average concentration at the outlet against the total cell number. Small concentration changes are negligible, increasing the number of cells from 441,408 to 660,000, 441,408 considered the best result. According to the statistics provided by COMSOL 5.6, the average element quality is 0.9912, the element volume ratio is 0.4187, and the mesh volume is 0.7916 cubic millimeters (mm³).

3. RESULTS AND DISCUSSION

3.1. Validation

For the model validation, simulation results were compared with numerical results presented by Shamloo et al.³³ Figure 3(a) illustrates the comparison of mixing quality against down-channel length in this numerical method and numerical results simulated by Shamloo et al.³³ These results are in good agreement with their results.

As shown in Figure 3(b), in the simulation performed by setting the values of voltage, frequency, and angular velocity of 5 (V), 12 (Hz), and 250 (rad/s), respectively, the mixing process is improved. The effective mixing length of 10 (mm), which was reported in Shamloo et al.³³ Simulation reduced to 5 (mm). This causes more patterns to be placed on the disk.

3.2. Effect of Different Parameters on M.Q.

3.2.1. Effect of Physical Parameters and Angular Velocity on M.Q.

According to Shamloo et al.,³⁷ no significant changes in the mixing quality are observed by changing the angle between two inlet channels. Also, in Ref. [33], microchannel curvature is investigated, which leads to an increase in dean flow, and subsequently, the mixing is improved. Figure 4(a) demonstrates concentration contour

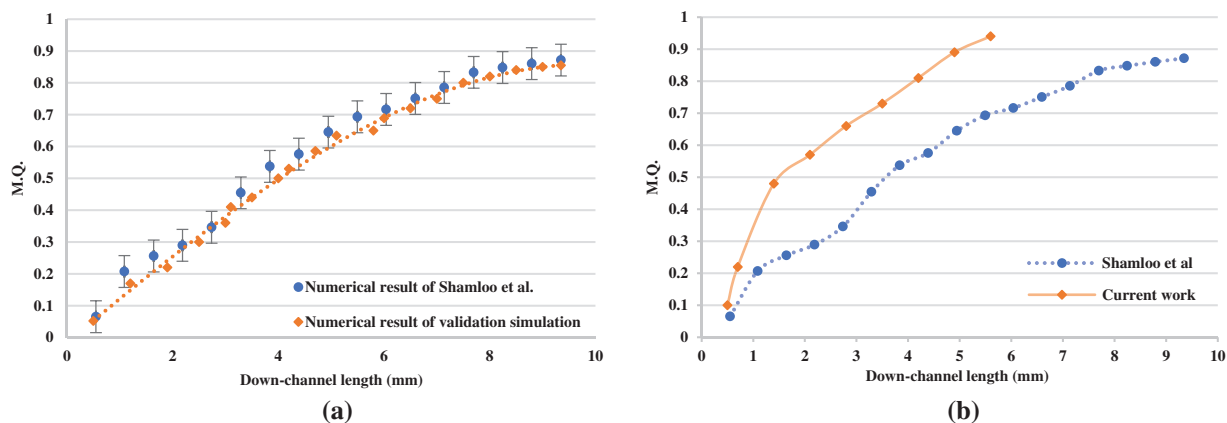


Fig. 3. Mixing quality versus down-channel length for: (a) validation analysis, (b) current simulation.

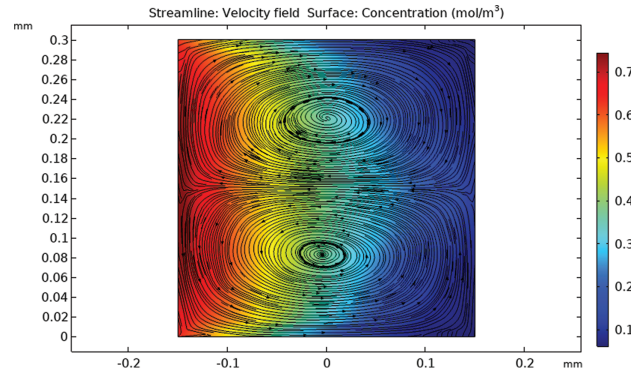


Fig. 4. Concentration contour and streamline at a cross-section at 10.7 mm distance from the center of rotation.

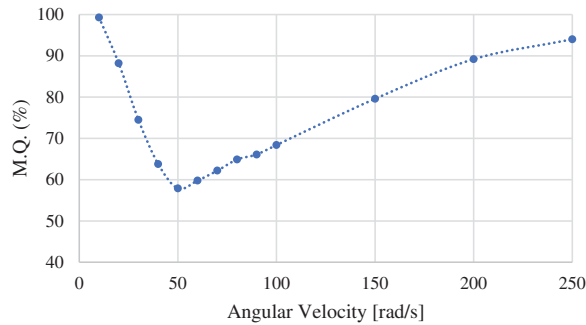


Fig. 5. Angular velocity effects on mixing quality.

and secondary flow streamlines at the cross-section in the distance of 10.7 (mm) from the center of rotation.

In the following section, the effect of angular velocity changes on the mixing quality is discussed. In order to study the effects of different angular velocities on the mixing quality from 10 to 250 (rad/s), the AC voltage and frequency are set to 5 (V) and 12 (Hz), respectively. Figure 4(b) depicts the results of the simulation.

As shown in Figure 5, increasing angular velocity from 10 up to 50 (rad/s) is associated with decreasing mixing quality, we also see an increase in mixing quality by increasing the angular velocity further than 50 (rad/s). It should be noted that in the figures where the mixing quality is reported versus parameters, the mixing quality at the outlet, which is 5 (mm), has been calculated.

Table II plots the result for the dimensionless Reynolds and Dean numbers against angular velocity across the investigated range. At the microchannel's outlet, all data was computed. By replacing $R_c = 350$ (μm) and $D_h = 300$ (μm) in: $De = Re\sqrt{D_h/2R_c}$, we have $De \cong 0.65Re$.

3.2.2. Effect of Voltage and Frequency Variation in the Electric Field on M.Q.

In order to investigate the effects of different voltages on mixing quality, AC voltage V_0 changes from 0 to 10 (V) while angular velocity and frequency are set to 250 (rad/s) and 12 (Hz), respectively. The results of these changes are

Table II. Evaluation of flow characteristics in relation to the angular velocity.

ω [rad/s]	Re	De	M.Q. (%)
10	0.048	0.0312	99.3
20	0.372	0.2418	88.2
30	0.912	0.5928	74.5
40	1.621	1.0536	63.8
50	2.31	1.5015	57.9
60	3.82	2.483	59.8
70	4.98	3.237	62.2
80	6.07	3.9455	64.9
90	7.64	4.966	66.1
100	8.91	5.7915	68.4
150	31.86	20.709	79.6
200	55.73	36.2245	89.2
250	45.86	29.809	94.31

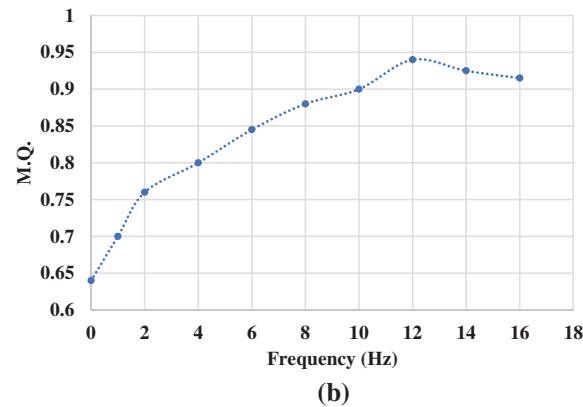
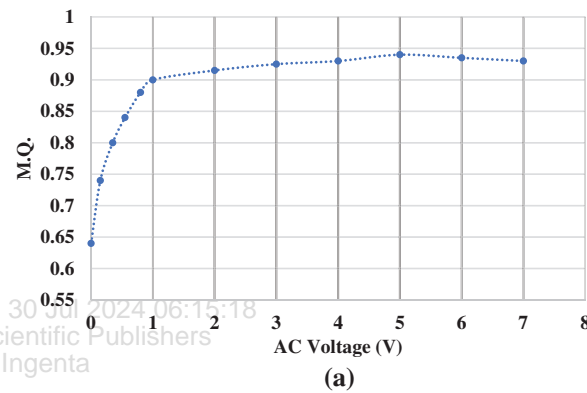


Fig. 6. Mixing quality variation with different (a) AC voltage, and (b) voltage frequency.

shown in Figure 6(a). Also, the angular velocity and voltage are adjusted to 250 (rad/s) and 5 (V), respectively, to explore the influence and connection between alternating field frequency and mixing efficiency. The frequency ranges between 0 and 16 (Hz).

Figure 6(a) demonstrates that the mixing quality increases significantly by increasing voltage from 0 to 1 (V). Increasing the voltage from 1 to 5 (V) increases the mixing quality at a lower rate than in the previous range. With increasing voltage from 5 volts, no significant

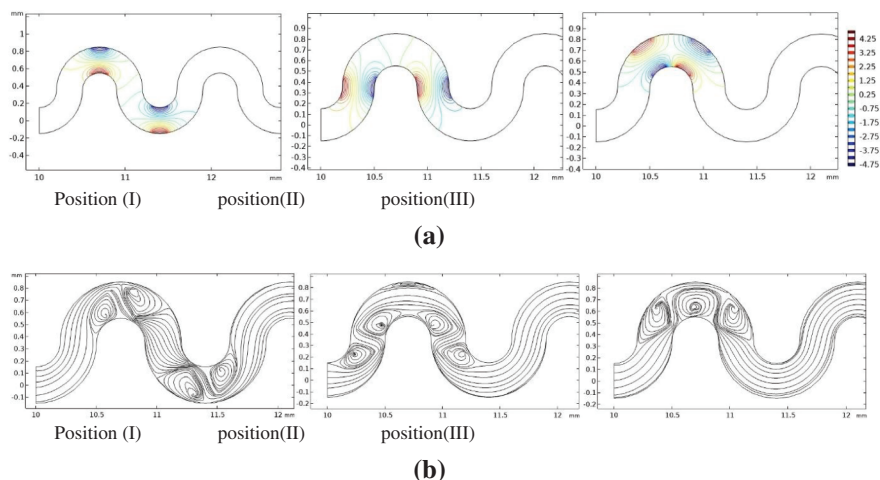


Fig. 7. (a) Three positions of two pairs of electrodes, (b) Fluid velocity streamline in a microchannel (Time = 0.21667 s).

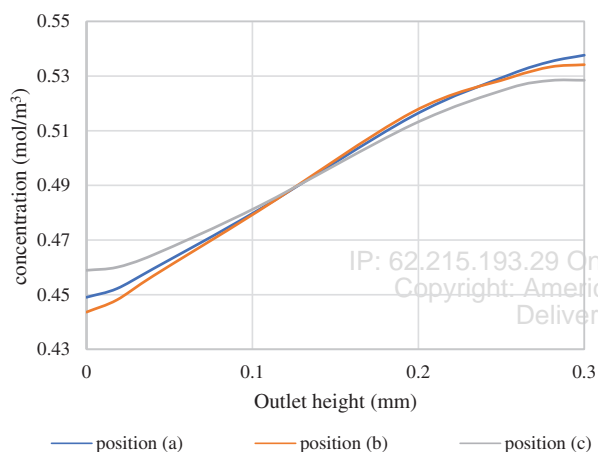


Fig. 8. Concentration at the outlet of the micromixer with different electrode positions.

increase in mixing efficiency is observed. Moreover, at 5 (V), the mixing quality is 94%.

Figure 6(b) depicts the simulation findings. The graph shows that the mixing efficiency improves as the frequency increases. The alternating electric field changes slowly when the frequency is low, resulting in the poor mixing efficiency of the solution. The best mixing efficiency is 94.3 percent when the frequency is 12 (Hz). Due to the

rapid fluctuations in the electric field, the longitudinal fluid velocity weakens during this period, and consequently, there is no further enhancement in the mixing efficiency of the solution.

3.2.3. Effect of the Electrode Pairs Position on M.Q.

Three distinct places, I, II, and III, were studied to establish the suitable position for electrode pairs, as illustrated in Figure 7(a). The electrodes' lengths are supposed to be identical; the angular velocity is 250 (rad/s), the voltage is 5 (V), and AC electric field is 12 (Hz). Figure 7(b) depicts the streamline for fluid flow in these three types.

In Figure 8, the influence of electrode placement on mixing quality is depicted. Upon comparing these three concentration graphs within a central cross-section of the outlet channel length, it is evident that the amalgamation of positive and negative electrodes enhances mixing efficiency. Consequently, due to the heightened concentration at the output, position (III) proves to be more effective than the other two.

3.2.4. Effect of the Electrode Pair Count on M.Q.

In order to assess how the quantity of electrode pairs influences mixing effectiveness, a set of face-to-face two-electrode pairs was employed. It was determined that using an electrode pair of identical dimensions, with a voltage

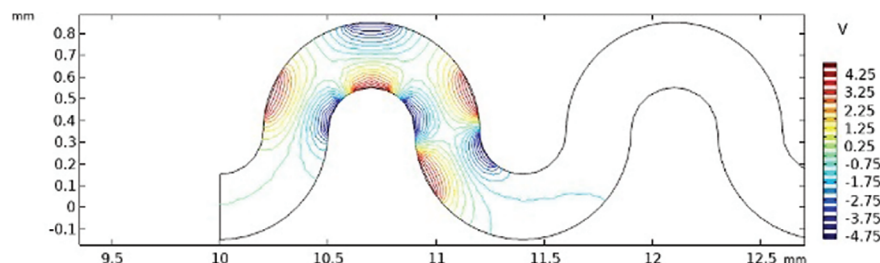


Fig. 9. Placement mode for four electrode pairs.

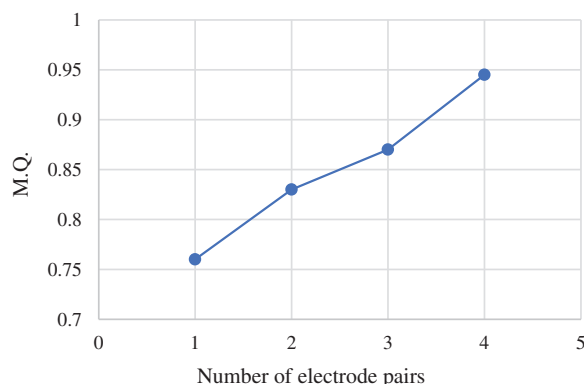


Fig. 10. Variation of *M.Q.* with the number of electrode pairs.

of 5 volts (V) and an alternating current frequency of 12 Hertz (Hz), would be appropriate. Furthermore, an angular velocity of 250 radians per second (rad/s) was maintained. The number of electrode pairs was incrementally raised from one to four. Figure 9 illustrates the placement of the electrode pair, while Figure 10 presents the corresponding mixing efficiency.

The efficacy of the mixer experiences a boost with each additional electrode pair. Concurrently, augmenting the number of electrode pairs leads to an increase in vortices within the channel. This significantly enlarges the region of fluid mixing and enhances lateral flow. The elevation of micromixer efficiency proves beneficial with an escalating number of electrode pairs.

4. CONCLUSION

The rotating microchannel is used in this research to present a novel form of active micromixer that enhances the mixing efficiency of the fluid in the microchannel. After doing several numerical simulation analyses, we obtained the following results: Microchannel curvature boosts the dean effect, resulting in secondary flow and better mixing.

An improvement in mixing efficiency of up to 94 percent can be achieved by adding an electric field. In addition, the efficient length it takes to attain this efficiency is cut in half, which means that more patterns are generated on the disk, which is important for diagnostic applications and chemical reactions. The critical rotational speed at which the dominant mixing mechanism transitions from diffusion to secondary flow is 50 (radians per second), as we have discovered. When secondary flow beyond this limit, diffusion loses out and mixing performance improves as angular velocity increases gradually. Augmented angular velocity induces a more vigorous secondary flow within areas post-threshold, culminating in superior mixing. The mixing quality at the channel output is improved by increasing the voltage and frequency in the geometry employed to 5 (V) and 12 (Hz), respectively. The number of electrode pairs and their placement were

also analyzed, and it was discovered that increasing the number increased the number of electrode pairs. To sum up, research has been done in order to reduce the space required by the mixing unit, which other operational units can be integrated for applications such as DNA sequencing and so on.

Funding Sources

No specific funding for this research was obtained from public, private, or nonprofit organizations.

Acknowledgments: Assistance provided by K. N. Toosi University Complex Fluid and Porous Media research lab team works was greatly appreciated.

References and Notes

1. H. A. Stone and S. Kim, *American Institute of Chemical Engineers. AIChE Journal* 47, 1250 (2001).
2. W. Han and X. Chen, *Journal of Chemical Technology & Biotechnology* 95, 1622 (2020).
3. S. Haeblerle and R. Zengerle, *Lab on a Chip* 7, 1094 (2007).
4. L. X. Kong, A. Perebikovskiy, J. Moebius, L. Kulinsky, and M. Madou, *Journal of Laboratory Automation* 21, 323 (2016).
5. J. Ducrée, S. Haeblerle, S. Lutz, S. Pausch, F. Von Stetten, and R. Zengerle, *Journal of Micromechanics and Microengineering* 17, S103 (2007).
6. Y. Ren and W. W. F. Leung, *Int. J. Heat Mass Transfer* 60, 95 (2013).
7. J. Xiang, Z. Cai, Y. Zhang, and W. Wang, *Sensors and Actuators B: Chemical* 259, 325 (2018).
8. M. Amasia and M. Madou, *Bioanalysis* 2, 1701 (2010).
9. G. Jia, Fast and automated DNA assays on a compact disc (CD)-based microfluidic platform (2006).
10. M. A. Kabir, H. Zilouchian, M. A. Younas, and W. Asghar, *Biosensors* 11, 206 (2021).
11. A. Dehghan, A. Gholizadeh, M. Navidbakhsh, H. Sadeghi, and E. Pishbin, *Sensors and Actuators B: Chemical* 351, 130919 (2022).
12. C. M. Miyazaki, E. Carthy, and D. J. Kinahan, *Processes* 8, 1360 (2020).
13. C. K. Su, *Anal. Chim. Acta* 1158, 338348 (2021).
14. N. Biswas, N. Kumar Manna, A. Mukhopadhyay, and S. Sen, *ASME. J. Fluids Eng.* 134, 011205 (2012).
15. H. Hajji, L. Kolsi, F. Askri, C. Maatki, W. Hassen, and M. N. Borjini, *Thermal Science* 25, 2483 (2021).
16. R. Ahmed, N. Ali, S. U. Khan, and I. Tlili, *AIP Advances* 10 (2020), DOI: 10.1063/5.0010964.
17. M. Bayareh, M. N. Ashani, and A. Usefian, *Chemical Engineering and Processing-Process Intensification* 147, 107771 (2020).
18. G. Cai, L. Xue, H. Zhang, and J. Lin, *Micromachines* 8, 274 (2017).
19. V. Ionescu, Numerical simulation of fluid flow on rotating microchannels for centrifugal micromixer applications, *IEEE EUROCON 2021-19th International Conference on Smart Technologies, IEEE*, July (2021), pp. 363–368.
20. V. Hessel, H. Löwe, and F. Schönfeld, *Chem. Eng. Sci.* 60, 2479 (2005).
21. W. Ruijin, L. Beiqi, S. Dongdong, and Z. Zefei, *Sensors and Actuators B: Chemical* 249, 395 (2017).
22. V. Goodarzi, S. H. Jafarbeygi, R. A. Taheri, M. Sheremet, and M. Ghalambaz, *Symmetry* 13, 915 (2021).
23. Z. Babaie, D. Bahrami, and M. Bayareh, *Meccanica* 57, 73 (2022).

24. E. Tripathi, P. K. Patowari, and S. Pati, *Chemical Engineering and Processing-Process Intensification* 169, 108609 (2021).
25. L. Chen, Y. Deng, T. Zhou, H. Pan, and Z. Liu, *Micromachines* 8, 105 (2017).
26. N. Sasaki, T. Kitamori, and H. B. Kim, *Anal. Sci.* 26, 815 (2010).
27. J. M. Park and T. H. Kwon, *ALChE J.* 54, 1999 (2008).
28. S. S. Wangikar, P. K. Patowari, and R. D. Misra, *Microsystem Technologies* 24, 3307 (2018).
29. V. E. Ahmadi, I. Butun, R. Altay, S. R. Bazaz, H. Alijani, S. Celik, M. E. Warkiani, and A. Koşar, *Chem. Eng. Res. Des.* 168, 490 (2021).
30. K. Karthikeyan and L. Sujatha, *International Journal of Chemical Reactor Engineering* 17, 20180047 (2018).
31. J. Steigert, M. Grumann, T. Brenner, K. Mittenbühler, T. Nann, J. Rühe, I. Moser, S. Haeberle, L. Riegger, J. Riegler, and W. Bessler, *JALA: Journal of the Association for Laboratory Automation* 10, 331 (2005).
32. M. La, S. J. Park, H. W. Kim, J. J. Park, K. T. Ahn, S. M. Ryew, and D. S. Kim, *Microfluidics and Nanofluidics* 15, 87 (2013).
33. A. Shamloo, P. Vatankhah, and A. Akbari, *Chemical Engineering and Processing: Process Intensification* 116, 9 (2017).
34. S. Xiong, X. Chen, and Y. Ma, *Journal of the Brazilian Society of Mechanical Sciences and Engineering* 43, 1 (2021).
35. S. Xiong and X. Chen, *International Journal of Chemical Reactor Engineering* 19, 97 (2021).
36. H. Jalili, M. Raad, and D. A. Fallah, *Proceedings of the Institution of Mechanical Engineers, Part C: Journal of Mechanical Engineering Science* 234, 2113 (2020).
37. A. Shamloo, M. Madadelahi, and A. Akbari, *Chemical Engineering and Processing: Process Intensification* 104, 243 (2016).

IP: 62.215.193.29 On: Tue, 30 Jul 2024 06:15:18
Copyright: American Scientific Publishers
Delivered by Ingenta